Journal of Molecular Catalysis A: Chemical 334 (2011) 108–115

Contents lists available at ScienceDirect

Journal of Molecular Catalysis A: Chemical

journal homepage: www.elsevier.com/locate/molcata

A DFT study on enantioselective synthesis of aza-β-lactams via NHC-catalyzed [2 + 2] cycloaddition of ketenes with diazenedicarboxylates

Donghui Wei, Yanyan Zhu*, Cong Zhang, Dongzhen Sun, Wenjing Zhang, Mingsheng Tang

Department of Chemistry, Center of Computational Chemistry, Zhengzhou University, 100# Kexuedadao Street, Zhengzhou, Henan 450052, China

ARTICLE INFO

Article history:
Received 17 June 2010
Received in revised form 19 August 2010
Accepted 8 November 2010
Available online 13 November 2010

Keywords:
Density functional theory (DFT)
N-Heterocyclic carbenes (NHC) catalyst
Ketenes-diazenedicarboxylates
cycloaddition

ABSTRACT

Recently, *N*-heterocyclic carbenes (NHCs) have been found to be efficient catalysts for the formal [2 + 2] cycloaddition of aryl(alkyl)ketenes and diazenedicarboxylates to give aza-β-lactams in good enantioselectivity (up to 91% ee) [X.-L. Huang, X.-Y. Chen, S. Ye, J. Org. Chem. 74 (2009) 7585–7587]. However, it is still ambiguous which step is the enantioselectivity-determining step and what the role of NHC catalysts is in this reaction. In this paper, we have suggested a possible mechanism of the title reaction and then theoretically investigated it in detail using density functional theory (DFT). Fully optimized geometries of reactants, products, transition states and intermediates were obtained at the B3LYP/[6-31G (d, p)/LANL2DZ] level of theory, and the results revealed that this reaction had three steps. Our calculated results indicate that the [2 + 2] cycloaddition step is the enantioselectivity-determining step. Moreover, the frontier molecular orbital (FMO) analysis has been carried out to explain why the NHC catalysts can make the [2 + 2] cycloaddition easier to occur, which is mainly due to that the energy gap of FMOs become narrower under the NHC-catalysis condition. Noteworthy, the results of global reactivity indexes analysis are consistent with those of the FMO analysis. Further calculations show that the solvent effect of dichloromethane has no great influence on enantioselectivity of this reaction.

1. Introduction

As the aza analogues of β-lactams, aza-β-lactams show some interesting biological activities [1,2] and are useful intermediates for the synthesis of R-amino acids and heterocyclic compounds [3,4]. Since Ingold and Weaver reported the first [2 + 2] cycloaddition of ketenes and diazenes to give aza-β-lactams [5–13], numerous methodologies for synthesis of aza-β-lactams have been developed over the past decades. Noteworthy, Taylor et al. were the main contributors for the synthesis and application of aza-β-lactams [14].

Nevertheless enantioselective [2 + 2] cycloaddition of ketenes and diazenes has been a challenge for many years. Due to the challenges involved in such endeavors and the applications of chiral aza-β-lactams in organic and medicinal chemistry, there has been great effort in designing and developing various kinds of chiral catalysts experimentally. For example, Berlin and Fu reported the first enantioselective [2 + 2] cycloaddition of ketenes with diazenedicarboxylates catalyzed by their planar–chiral 4-pyrrolidinopyridine derivatives [15].

Recently, *N*-heterocyclic carbenes (NHCs) were found to be efficient catalysts for the enantioselective cycloaddition between ketenes and C=O (or C=N, N=N) bond [16]. For example, Ye et al. reported that the highly enantioselective synthesis of lactones can be obtained by chiral NHC-catalyzed formal cycloaddition reaction of alkyl(aryl)ketenes and trifluoromethyl ketones [16a,b]. NHCs were also demonstrated to be efficient catalysts for the Staudinger reaction of ketenes with *N*-tosyl, *N*-benzyloxycarbonyl, or *N*-tert-butoxycarbonyl imines [16c]. Connected to the above, it is worth mentioning that NHCs had been used for promoting the formal [2 + 2] cycloaddition aryl(alkyl) ketenes and diazenedicarboxylates to give the corresponding aza-β-lactams in good yields with up to 91% ee [16g]. However, no report of theoretical investigations about the mechanism of this reaction has been found by now. Thus, it is still ambiguous which step is the enantioselectivity-determining step and which factor is the decisive factor on enantioselectivity in this reaction. In addition, it is also essential to make clear why the reaction can occur more easily and has a good enantioselectivity under the NHC-catalysis condition.

Noteworthy, Yamabe et al. had provided the precise frontier molecular orbital (FMO) pictures for the [2 + 2] cycloaddition of ketene and C=X (X=O, NH, and CH_2) bond under non-catalysis condition [17], but it is still unknown whether there is a same overlap mode of the frontier molecular orbitals under the NHC-catalysis condition in the past decades. All of the questions mentioned above prompted us not only to investigate the mechanisms of the title reaction, but also to give a deep investigation on the frontier molecular orbital interactions. As described above, we think this work

* Corresponding author. Tel.: +86 371 67767051; fax: +86 371 67767051.
E-mail addresses: zhuyan@zzu.edu.cn (Y. Zhu), mstang@zzu.edu.cn (M. Tang).

1381-1169/$ – see front matter © 2010 Elsevier B.V. All rights reserved.
doi:10.1016/j.molcata.2010.11.004

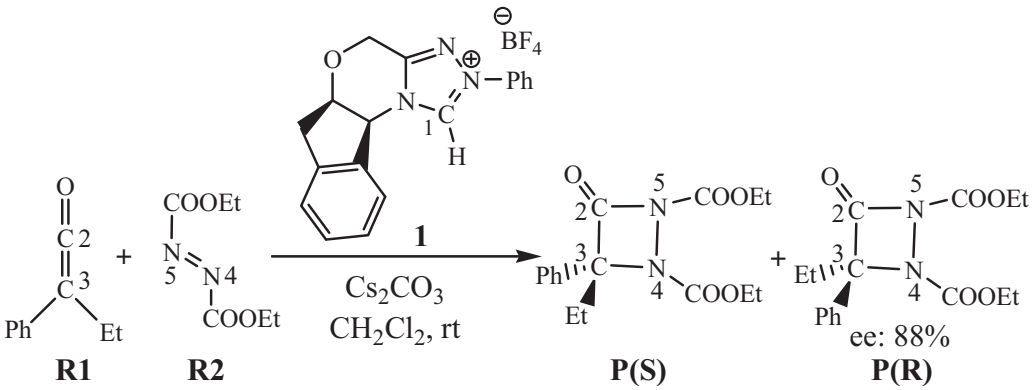

Scheme 1. The [2 + 2] cycloaddition catalyzed by NHC 1.16 g.

should help explaining how the NHC catalyst work and what the role of NHC catalyst is, which should be certainly helpful for the new catalysts and novel catalyzed reaction designs.

In this project, the [2 + 2] cycloaddition of **R1** and **R2** promoted by catalyst 1 to give **P(R)** with 88% ee (Scheme 1) has been chosen as the objects of investigation, which was uniform with the experimental work (X.-L. Huang, X.-Y. Chen, S. Ye, J. Org. Chem. 74 (2009) 7585–7587). And the reaction mechanisms were studied using density functional theory, which has been widely used in the studies of the mechanisms [18–21].

2. Computational details

All theoretical calculations were performed using the Gaussian 03 [22] suite of programs. The geometrical structures of all the stationary points in energy profiles were optimized by employing the hybrid density functional B3LYP method [23,24] and Cs atom was modeled by a LANL2DZ, while 6–31G (d, p) basis set was used for all other atoms. The corresponding vibrational frequencies were calculated at the same level to take account of the zero-point vibrational energy (ZPVE) and to identify the transition states. We had confirmed that all reactants and intermediates had no imaginary frequencies, and each transition state had one, and only one, imaginary frequency. The intrinsic reaction coordinate (IRC) calculations [25,26], at the same level of theory, were performed to ensure that the transition states led to the expected reactants and products. Moreover, frontier molecular orbital analysis and NBO charge had been performed at the B3LYP/6-31G (d, p) level.

Finally, the solvent effect had been considered in this paper. Based on our computational works [18a,b], we think solvent effect of the enantioselectivity-determing step could be important for this type of reaction. Therefore, we had optimized the geometries and calculated the corresponding vibrational frequencies of the two transition states **TS2′(S)**, **TS2′(R)** and the two intermediates **M2′(S)**, **M2′(R)** in dichloromethane at the B3LYP/6-31G (d, p) level using the integral equation formalism polarizable continuum model (IEF-PCM) method [27,28].

3. Results and discussion

3.1. Reaction mechanisms of the title reaction

According to our calculations, we believe the reaction proceed via the following mechanism (Scheme 2).

All compounds shown in Scheme 2 will be referred to by their associated number for the sake of brevity. Initially 1 is converted successfully into **1a** (as can be seen in Scheme 2, **1a** is the true catalyst) [16g]. The following processes, starting with the reaction between **1a** and ketene **R1**, and then with **R2**, are the focus of our investigation. The corresponding representation of the energy profile is illustrated in Fig. 1. As shown in Fig. 1, we set the energies (E + ZPVE) of **R1** + **R2** + **1a** as 0.00 kcal/mol as reference in the potential energy profiles.

We begin by studying the chemical combination of **1a** with **R1**. **1a** can initiate the reaction through **(E&Z)-TS1** (Fig. 2), which results from the approach of **1a** to the ketene and leads to the complex **(E&Z)-M1**. For the double bond C2=C3, **(E)-M1** and **(Z)-M1** are a pair of E and Z-isomers. The distances of C1–C2 are 2.452 Å in **(E)-TS1** and 2.484 Å in **(Z)-TS1**, which are shortened to 1.512 Å in **(E)-M1** and 1.511 Å in **(Z)-M1** (Fig. 2), respectively.

As can be seen from Table 1, the values of NBO charge on the C1 and C2 atoms from **1a** and **R1** to the zwitterion **(E&Z)-M1** changed drastically, which was mainly due to the new C1–C2 bond formation. Apart from the above, the charge value of N6 atom changes from −0.253 e in **1a** to −0.173 e in **(E)-M1** (0.169 e in **(Z)-M1**), which indicates that the N6 atom become a positive charge center in **(E&Z)-M1**. At the same time, the charge value of O7 atom changes from −0.437 e in **1a** to −0.711 e in **(E)-M1** (−0.715 e in **(Z)-M1**), showing that O7 becomes a negative charge center in the **(E&Z)-M1**, thus, the intermediates **(E)-M1** and **(Z)-M1** should be zwitterions. Obviously, there is a charge transfer process from catalyst **1a** to the reactant **R1** in this step. The energy barriers of the first step are 2.44 kcal/mol (E) and 2.10 kcal/mol (Z) (Fig. 1), respectively. Moreover, **(E)-M1** lies 15.67 kcal/mol below the energy of the reactants, while **(Z)-M1** lies 17.29 kcal/mol below the energy of the reactants. What we have described above indicates that the interaction of carbene carbon atom C1 and the C2 of the ketene stabilize the resulting complexes **(E&Z)-M1**.

The second step is a formation of four-membered ring (C2–C3–N4–N5) through the [2 + 2] cycloaddition. In this step, **R2** could form the intermediates **M2(S&R)** (Fig. 3) with **(E&Z)-M1** by weak interactions. M2(S) and M2(R) are the reaction precursors. The N4 atom attacks to the prochiral carbon atom C3 in M2(S&R), corresponding to the N4 atom attacking the *Si* face and *Re* face of the ketene, and produces two diastereotopic transition states **TS2(R)** and **TS2(S)** (Fig. 3), respectively. After the bond C3–N4 is formed, the single bond C2–N5 is also generated in **M3(S&R)** (Fig. 4) via **TS2(S&R)**, so the [2 + 2] cycloaddition is a concerted reaction.

The distances of C2–C3, C3–N4, N4–N5, C2–N5 in **M2(S&R)**, **TS2(S&R)** and **M3(S&R)** are summarized in Table 2. The distances of C2–N5 and C3–N4 are shortened from 3.001 Å and 2.929 Å in the structure of **M2(S)** to 2.804 Å and 2.059 Å in **TS2(S)**, respectively. While the distances of C2–N5 and C3–N4 are shortened from 3.060 Å and 3.126 Å in the structure of **M2(R)** to 2.707 Å and 1.899 Å in **TS2(R)**. The energy of **TS2(S)** is 4.13 kcal/mol higher than that of the reactants, and **TS2(S)** leads to intermediate **M3(S)** which has an *S* configuration at the chiral center C3 atom. **TS2(R)** leads to the *R* configuration, **M3(R)**, and the newly formed C2–N5 and

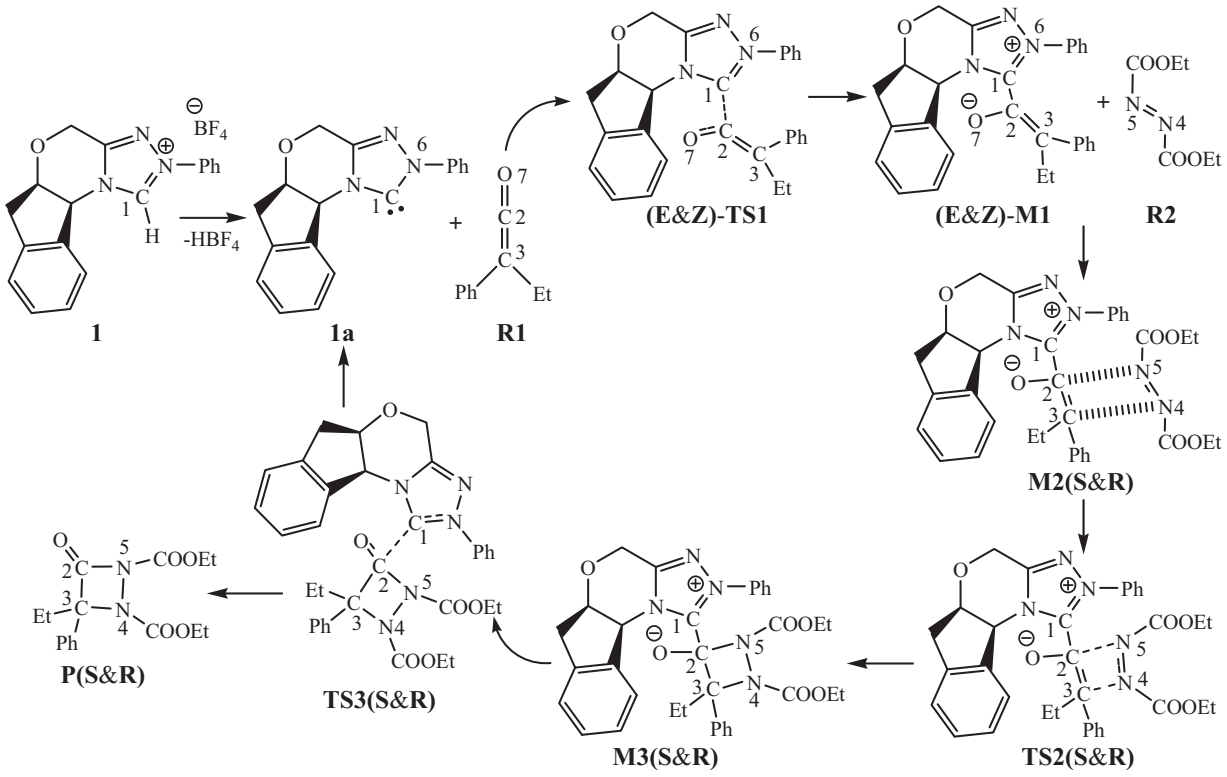

Scheme 2. The overall reaction mechanism.

C3–N4 bond are 1.661 Å and 1.464 Å separately. The difference in energy between **TS2(S)** and **TS2(R)** is due to the different amount of repulsion with **R2** gradually close to **(E&Z)-M1**.

The energy barrier for ring formation is 18.46 kcal/mol via **TS2(S)** compared to 16.29 kcal/mol via **TS2(R)**. Noteworthy, this step has the highest energy barrier in energy profile and the C3 atom will become a chiral center via **TS2(S&R)**. The ΔG we have calculated for this step is 20.69 kcal/mol for the *S* configuration and 17.87 kcal/mol for the *R* configuration, respectively, the highest energy barrier among the reaction steps. Furthermore, the energy barrier of **P(S&R)** + 1a through **TS2(S&R)** is so high (41.63 kcal/mol (*S*) and 35.12 kcal/mol (*R*), Fig. 1) that the reaction is clearly irreversible at room temperature. Hence the energy barrier of this step will be crucial for determining the stereochemical outcome of the reaction. Moreover, we find that the benzene in ketene and that in catalyst are stacked in *R* configuration, therefore, there should be a π–π weak interactions between them, which is one reason of making the *R* configuration more energy favorable.

The difference of ΔE between *S* and *R* configuration in this step is 2.17 kcal/mol (Fig. 1). This value would correspond to an enantiomeric excess of about 94% [18a,b], which approximately predicts the experimental outcome (88% ee). Thus, it provides the correct stereochemical preference of the reaction, in agreement with the experimental result.

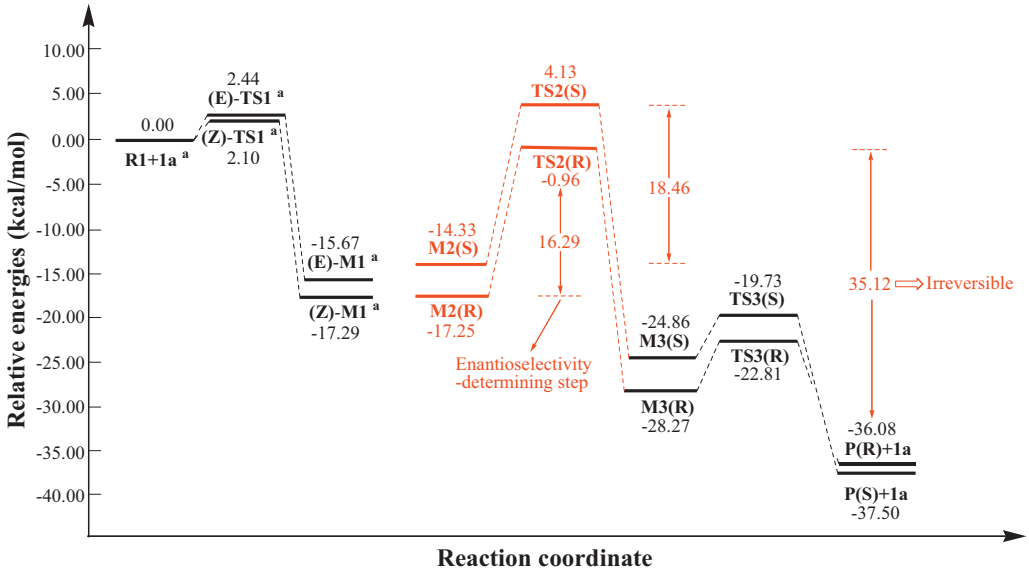

Fig. 1. Potential energy profiles for the whole reaction along the reaction coordinate (unit: kcal/mol, the superscript a represents adding the energy of **R2**).

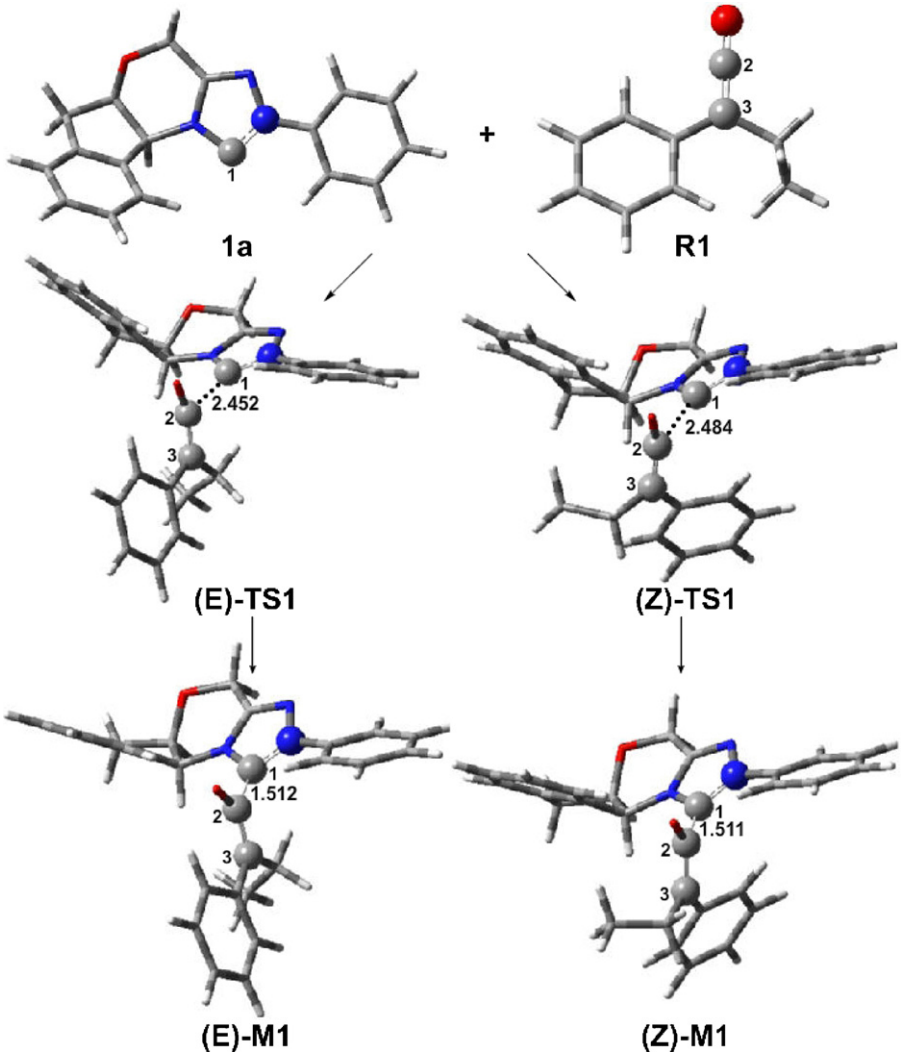

Fig. 2. Optimized structures of the critical points reactants (**1a** and **R1**), **(E&Z)-TS1** and **(E&Z)-M1** (units in Å for bond lengths).

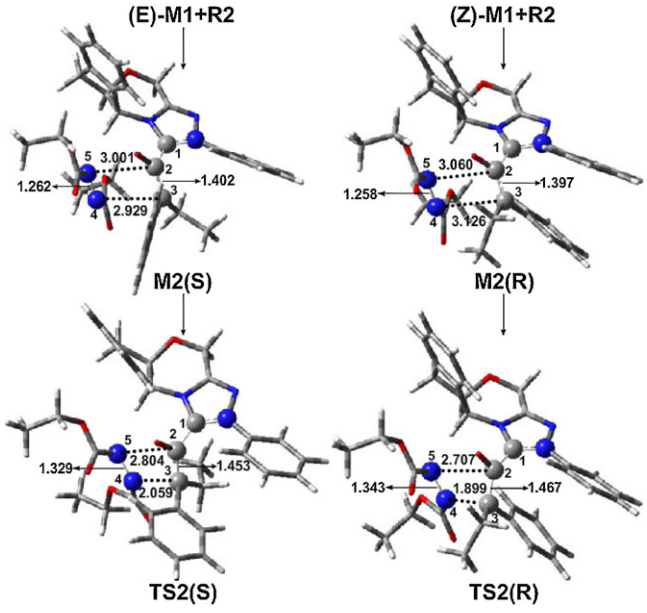

Fig. 3. Optimized structures for **M2(S&R)** and **TS2(S&R)** (units in Å for bond lengths).

In the last process of the reaction we are concerned, catalyst 1a is released by breaking the C1–C2 bond through the transition state **TS3(S&R)** (Fig. 4). The C1–C2 bond lengthens to 2.030 Å in **TS3(S)** and 2.067 Å in TS3(R), respectively. The energies of **P(S&R)** + **1a** are 37.50 and 36.08 kcal/mol lower than that of the reactants, therefore, the overall reaction is an exothermic process. Further, the energy barrier through TS3(S&R) is 5.13 and 5.46 kcal/mol, so the C1–C2 bond in **M3(S&R)** will be broken easily leading to **P(S&R)** and **1a**.

In addition, we have calculated a similar mechanism by the use of a model composed of **1a**(carbene), **R1**(ketene) and Cs^+ (Cs atom was modeled by a LANL2DZ, and 6–31G (d, p) basis set was used for all other atoms) as follows (Scheme 3).

As can be seen from Scheme 3, we have optimized all the structures of the stationary points with the cation Cs^+ and provided their cartesian atomic coordinates in Supplementary data.

Table 1
The values of NBO charge on the C1, C2, N6 and O7 atoms in **R1**, **1a**, **(E)-M1** and **(Z)-M1** at the B3LYP/6-31G (d, p) level (unit: e).

	C1	C2	C3	N6	O7
R1	–	0.716	−0.315	–	−0.437
1a	0.136	–	–	−0.253	–
(E)-M1	0.476	0.303	−0.169	−0.173	−0.711
(Z)-M1	0.476	0.308	−0.173	−0.169	−0.715

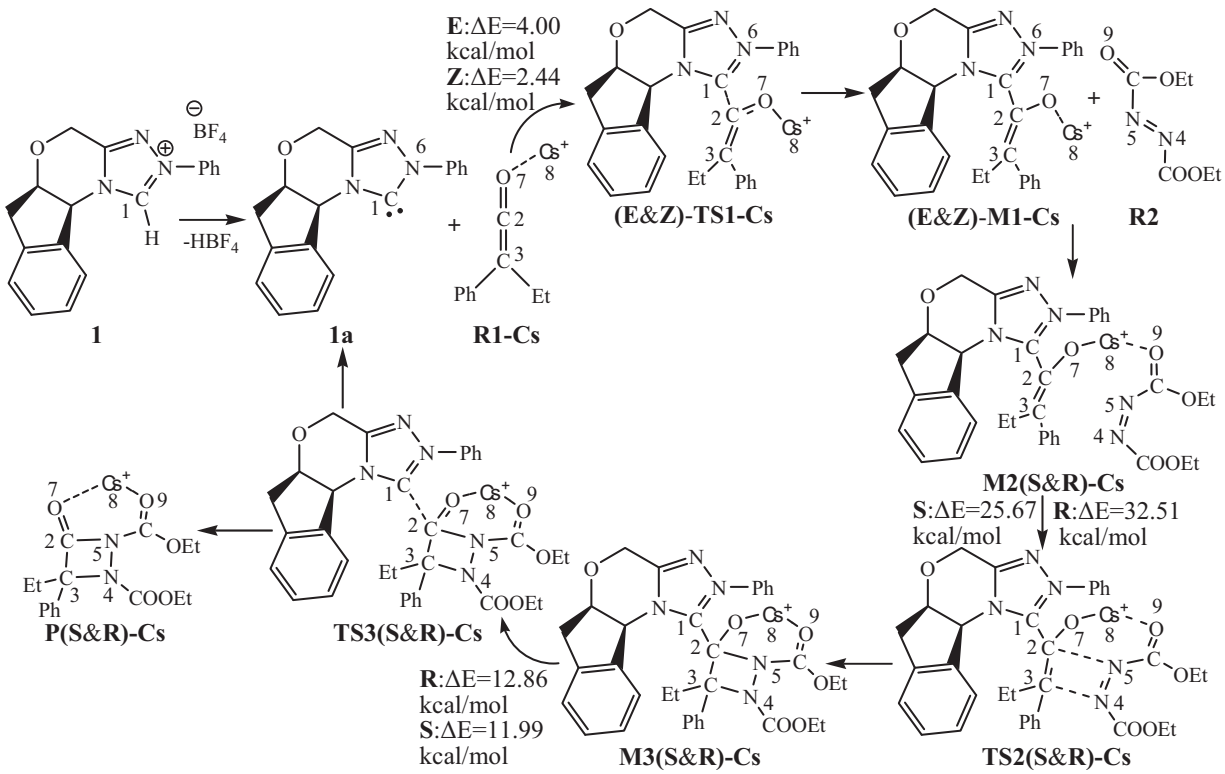

Scheme 3. The overall reaction mechanism with the cation Cs^+.

The energy barriers of the three steps are summarized in Scheme 1, and it is obvious that the energy barrier of the [2+2] cycloaddition process is also the highest among these of the three steps. Moreover, the energy barriers of the [2+2] cycloaddition processes with the cation Cs^+ are 32.51 kcal/mol (R) and 25.67 kcal/mol (S), which are higher than those of the mechanism with no cation Cs^+ (16.29 kcal/mol (R) and 18.46 kcal/mol (S)), thus, we think the mechanism without the cation Cs^+ should be more energy favorable than that with the cation Cs^+.

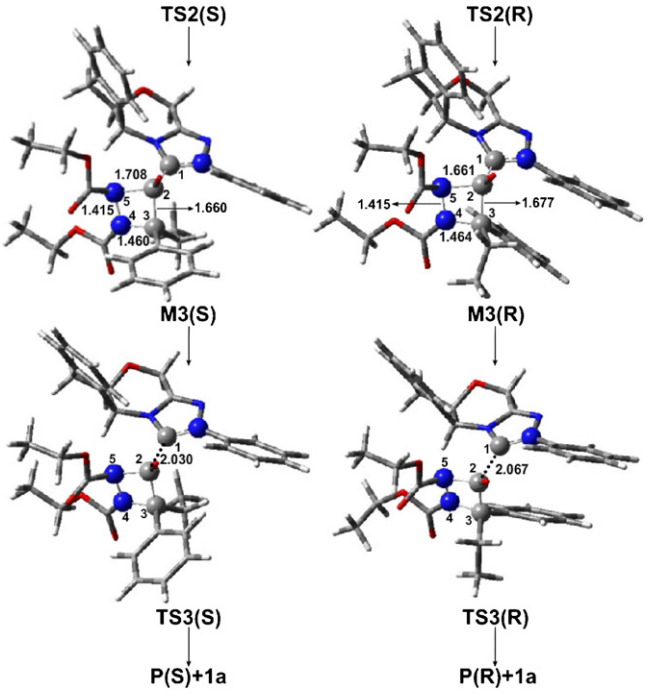

Fig. 4. Optimized structures of TS3(S&R) and **M3(S&R)** (units in Å for bond lengths).

3.2. Frontier molecular orbital analysis

In order to explore the role of NHC catalyst in this reaction, the frontier molecular orbital analysis on the process of [2+2] cycloaddition has been carried out in this paper. Noteworthy, Yamabe et al. have carefully investigated the orbital interactions of [2+2] cycloaddition between ketene and C=X (X=O, NH, and CH_2) bond under non-catalysis condition [17]. We have also investigated the reaction mechanisms of ketene–ketone [2+2+2] cycloaddition to form 3-aryglutaric anhydrides under a Lewis acid catalysis, and have found that the overlap mode of the frontier molecular orbitals under the Lewis acid catalysis is different from that under non-catalyzed condition in the process of [2+2] cycloaddition [18e]. Actually, the overlap mode of the frontier molecular orbitals under the NHC-catalysis condition is also different from that under the non-catalysis condition, which mainly due to formation of the C1–C2 bond, this would be an important reason for lowering the energy barrier of [2+2] cycleoaddition (see Ref.

Table 2
Some geometrical parameters of several SP (stationary points) along the reaction coordinate (units in Å for bond lengths).

SP	C1–C2	C2–C3	C3–N4	N4–N5	C2–N5
M2(S)	1.501	1.402	2.929	1.262	3.001
M2(R)	1.501	1.397	3.126	1.258	3.060
TS2(S)	1.523	1.453	2.059	1.329	2.804
TS2(R)	1.511	1.467	1.899	1.343	2.707
M3(S)	1.556	1.660	1.460	1.415	1.708
M3(R)	1.552	1.677	1.464	1.415	1.661
M2′(S)	1.508	1.404	2.935	1.265	2.999
M2′(R)	1.504	1.397	3.107	1.261	3.045
TS2′(S)	1.523	1.462	2.065	1.336	2.807
TS2′(R)	1.517	1.468	1.943	1.344	2.732

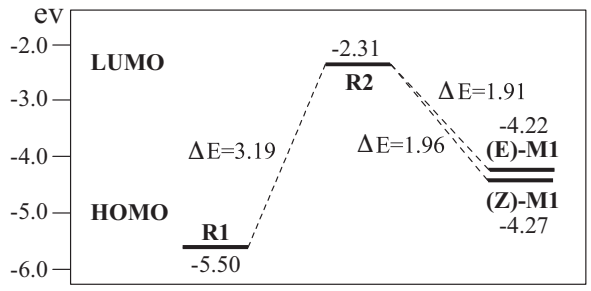

Fig. 5. The calculated frontier molecular orbitals of **R1**, **R2**, **(E)-M1** and **(Z)-M1** at the B3LYP/6-31G (d, p) level (unit: eV). The ΔE value is the difference between HOMO and LUMO.

[18e]). Based on these researches and the pictures of frontier molecular orbitals (FMO), we find that the orbital interactions mainly begin to occur between $LUMO_{R2}$ and $HOMO_{(E)\text{-}M1}$ (or $HOMO_{(Z)\text{-}M1}$) under the NHC-catalysis condition in this step, which are the interactions of $LUMO_{R2}$ and $HOMO_{R1}$ under non-catalysis condition correspondingly. The orbital pictures of the $HOMO_{R1}$, $LUMO_{R2}$, $HOMO_{(E)\text{-}M1}$ and $HOMO_{(Z)\text{-}M1}$ calculated at the B3LYP/6-31G (d, p) level have been represented in Fig. S1, which has been provided in supplementary data.

As shown in Fig. 5, the energy gap of $LUMO_{R2}$ and $HOMO_{R1}$ is 3.19 eV, while the energy gap of $LUMO_{R2}$ and $HOMO_{(E)\text{-}M1}$ (or $HOMO_{(Z)\text{-}M1}$) is 1.91 eV (or 1.96 eV), which indicates that the energy gap has become narrow under the NHC-catalysis condition, this fact explain why the reaction has a lower energy barrier under the NHC-catalysis condition than that of reaction under non-catalysis condition [29]. Although the energy gap of $LUMO_{R2}$ and $HOMO_{(Z)\text{-}M1}$ is wider than that of $LUMO_{R2}$ and $HOMO_{(E)\text{-}M1}$, the *R* configuration (corresponding to the reaction of **R2** and **(Z)-M1**) is more energy favorable than the *S* configuration (corresponding to the reaction of **R2** and **(E)-M1**), which seems to be that the enantioselectivity has little relationship with the energy gaps. Thus, we think that the steric effect between **R2** and **(Z)-M1** (or **(E)-M1**) have more influence than the energy gap between them on the enantioselectivity of this reaction. Furthermore, the DFT/B3LYP method has been widely and successfully used in describing weak interactions and explaining the enantioselectivity of catalyzed reactions [18a,b], however, there are not many obvious evidences to indicate that the steric effect between reactants and catalyst would be crucial for the enantioselectivity except discussing the structures in theory, so this paper gives a reasonable evidence in a different perspective using the DFT/B3LYP method.

3.3. Analysis of the global reactivity indexes of the reactants in the [2+2] cycloaddition step

As can be seen in Table 3, the molecule global electrophilicity character is measured by electrophilicity index [30a], ω, which has be given from the following expression, $\omega = (\mu^2/2\eta)$ [30a–e], in terms of the electronic chemical potential μ and the chemical hardness η. Both quantities may be approached in terms of the one-electron energies of the frontier molecular orbital HOMO and LUMO, E_H and E_L, as $\mu \approx (E_H + E_L)/2$ and $\eta \approx (E_L - E_H)$. Moreover, according the HOMO energies obtained within the Kohn–Sham scheme [30d], Domingo and co-workers gave the nucleophilicity index N to handle a nucleophilicity scale [30e–i]. The nucleophilicity index is defined as $N = E_{HOMO(SR)} - E_{HOMO(TCE)}$. This nucleophilicity scale is referred to tetracyanoethylene (TCE) taken as a reference. Followed these indices definition, in this reaction, **R2** is classified as the electrophile ($N = 2.638$ eV). **R1**, **(E)-M1**, **(Z)-M1** are the nucleophiles with the value of 3.808 eV, 5.249 eV and 5.195 eV, respectively. The nucleophiles value of **(E)-M1**, **(Z)-M1** are obviously larger than **R1**, indicating that coordination of NHC to the ketene carbon atom of **R1** noticeably increases the nucleophilicity of the corresponding complex of **(E)-M1** and **(Z)-M1**, and decreases the energy barrier of [2+2] cycloaddition, which is in good agreement with the results of FMO analysis.

Table 3
Energy of HOMO (E_H, a.u.), energy of LUMO (E_L, a.u.), electronic chemical potential (μ, in a.u.), chemical hardness (η, in a.u.), global electrophilicity (ω, in eV) and global nucleophilicity (N, in eV) of some reagents (SR) involved in the [2+2] cycloaddition step.

SR	E_H (a.u.)	E_L (a.u.)	μ (a.u.)	η (a.u.)	ω (eV)	N (eV)
R2	−0.251	−0.085	−0.168	0.166	2.312	2.638
R1	−0.202	−0.036	−0.119	0.166	0.161	3.808
(E)-M1	−0.155	−0.048	−0.1015	0.107	1.306	5.249
(Z)-M1	−0.157	−0.049	−0.103	0.108	1.306	5.195

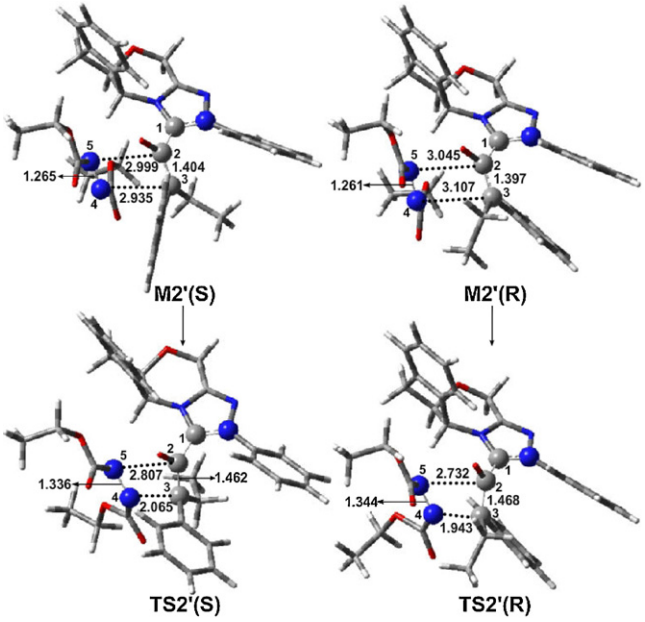

Fig. 6. Optimized structures of **M2′(S&R)** and **TS2′(S&R)** (units in Å for bond lengths).

As all we known, ketenes are usually electrophilic reagents, however, the present ketene would work as a nucleophilic one toward the N=N bond. In order to make the donor–acceptor relation clear, we have calculated the energy barrier of the [2+2] step by the use of the dichloroketene ($Cl_2C{=}C{=}O$) (no R&S configuration), which is higher than those of the ethyl phenyl ketene (16.29 kcal/mol (R) and 18.46 kcal/mol (S)), therefore, it is true that the dichloroketene is typically electrophlic and would be of poorer reactivity than ethyl phenyl ketene in this reaction. The cartesian atomic coordinates of **M2-Cl** and **TS2-Cl** have been provided in Supplementary data.

3.4. Solvent effects

The solvent effect of dichloromethane on the enantioselectivity of this reaction was also taken into account. Because the second step is the enantioselectivity-determing step, the two transition states **TS2(S&R)** and two transition states **M2(S&R)** have been optimized in dichloromethane, at the B3LYP/6-31G (d, p) level using the IEF–PCM method by means of geometrical optimizations. Although the solvent effect will affect the other reaction steps, we think solvent effect of the enantioselectivity-determing step could be representative for this type of reaction [18a]. The structures of **TS2(S&R)** and **M2(S&R)** are **TS2′(S&R)** and **M2′(S&R)**, respectively,

which are represented in Fig. 6 and Table 2. The energy barrier for [2 + 2] cycloaddition is 15.66 kcal/mol via **TS2′(S)** compared to 14.55 kcal/mol via **TS2′(R)**. By comparing the structures and the energy barriers in gas phase and in solvent, we find the differences are tiny, which demonstrates that the solvent has little influence on the reaction.

4. Conclusions

In this paper, an integrated mechanism for the catalytic cycle has been investigated using density functional theory (DFT). The calculated results revealed that this reaction should take place via three steps: initially **1a** approaches the carbonyl group of the ketene and forms an intermediate **(E&Z)-M1**. The second step is a [2 + 2] cycloaddition, which can occur via two different pathways, and each has a diastereaotopic transition state. One pathway corresponds to attacking of the ketene at the *Si* face while the other pathway involves attacking at the *Re* face. Our calculations indicated the stereoisomer with configuration *R* at the new chiral center is more energetically favorable. The energetic favorability of the *R* configuration stereoisomer suggests that it should be the dominant product, which is in good agreement with experiment. In addition, as shown by the potential energy profile (Fig. 1), the transition states **TS2(S&R)** are key for stereoselectivity. The remaining steps involve release of the catalyst **1a**. In addition, the results of test calculations on the mechanism with the cation Cs^+ have been compared with the above mechanism, which demonstrates that the mechanism without the cation Cs^+ should be more energy favorable in the potential energy profiles.

Moreover, the frontier molecular orbital analysis indicates that the energy gap of FMO will be narrower under the NHC-catalysis condition, and the steric effect will determine the enantioselectivity of this reaction. Actually, we think there are two reasons for the NHC catalyst to make the reaction more easily to occur. First, the NHC changes the overlap mode between the FMOs of **R1** and **R2**, which is similar with the catalyst BF_3 and this has been proved in our reference [18e]. Second, the energy gap between $HOMO_{R1}$ and $LUMO_{R2}$ is reduced under the NHC catalysis, which has been discussed in this work. Noteworthy, the results of global reactivity indexes analysis are consistent well with those of FMO analysis. In addition, the calculations also indicate that the solvent effect of dichloromethane has tiny influence on the enantioselectivity of this reaction. This study provides a model for predicting the enantioselectivity of the product, which should be helpful in designing other enantioselective catalysts.

Acknowledgments

The work described in this paper was supported by the National Natural Science Foundation of China (nos. 20873126, 20673011, 20631020, 20771017 and 20973024).

Appendix A. Supplementary data

Cartesian atomic coordinates and the ZPVE, E, H, G of all the reactants, intermediates, transition states, and products obtained using the DFT/B3LYP method. Moreover, the Cartesian atomic coordinates of **TS2′(S&R)** and **M2′(S&R)** optimized at the same level in the solvent CH_2Cl_2 using IEF-PCM method had been provided. In addition, the orbital pictures of the $HOMO_{R1}$, $LUMO_{R2}$, $HOMO_{(E)\text{-}M1}$ and $HOMO_{(Z)\text{-}M1}$ (Fig. S1) had also been represented in Supplementary data. Supplementary data associated with this article can be found, in the online version, at http://www.sciencedirect.com. Supplementary data associated with this article can be found, in the online version, at doi:10.1016/j.molcata.2010.11.004.

References

[1] H. Morioka, M. Takezawa, H. Shibai, T. Okawara, M. Furukawa, Agric. Biol. Chem. 50 (1986) 1757–1764.
[2] S.A. Abdel-Ghaffar, G.B. Mpango, M.A. Ismail, S.K. Nanyonga, Boll. Chim. Farm. 141 (2002) 389–393.
[3] H. Vogt, S. Brase, Org. Biomol. Chem. 5 (2007) 406–430.
[4] C. Cativiela, M.D. Diaz-de-villegas, Tetrahedron Asymmetry 18 (2007) 569–623.
[5] C.K. Ingold, S.D. Weaver, J. Chem. Soc. 127 (1925) 378–387.
[6] (a) T.T. Tidwell, Ketenes, Wiley–Interscience, NewYork, 2006;
(b) T.T. Tidwell, Angew. Chem. Int. Ed. 44 (2005) 5778–5785;
(c) T.T. Tidwell, Eur. J. Org. Chem. (2006) 563–576.
[7] B. List, J. Am. Chem. Soc. 124 (2002) 5656–5657.
[8] A. Bogevig, K. Juhl, N. Kumaragurubaran, W. Zhuang, K.A. Jørgensen, Angew. Chem. Int. Ed. 41 (2002) 1790–1793.
[9] N. Kumaragurubaran, K. Juhl, W. Zhuang, A. Bogevig, K.A. Jørgensen, J. Am. Chem. Soc. 125 (2003) 6254–6255.
[10] M. Marigo, K. Juhl, K.A. Jørgensen, Angew. Chem. Int. Ed. 42 (2003) 1367–1369.
[11] S. Saaby, M. Bella, K.A. Jørgensen, J. Am. Chem. Soc. 126 (2004) 8120–8121.
[12] Y. Hasegawa, W. Watanabe, I.D. Gridnev, T. Ikariya, J. Am. Chem. Soc. 130 (2008) 2158–2159.
[13] R. He, X. Wang, X. Wang, T. Hashimoto, K. Maruoka, Angew. Chem. Int. Ed. 47 (2008) 9466–9468.
[14] (a) E.C. Taylor, R.J. Clemens, H.M.L. Davies, N.F. Haley, J. Am. Chem. Soc. 103 (1981) 7659–7660;
(b) E.C. Taylor, H.M.L. Davies, R.J. Clemens, H. Yanagisawa, N.F. Haley, J. Am. Chem. Soc. 103 (1981) 7660–7661;
(c) E.C. Taylor, N.F. Haley, R.J. Clemens, J. Am. Chem. Soc. 103 (1981) 7743–7752;
(d) E.C. Taylor, R.J. Clemens, H.M.L. Davies, J. Org. Chem. 48 (1983) 4567–4571;
(e) E.C. Taylor, H.M.L. Davies, W.T. Lavell, N.D. Jones, J. Org. Chem. 49 (1984) 2204–2208;
(f) E.C. Taylor, H.M.L. Davies, J.S. Hinkle, J. Org. Chem. 51 (1986) 1530–1536;
(g) E.C. Taylor, H.M.L. Davies, J. Org. Chem. 51 (1986) 1537–1540;
(h) E.C. Taylor, J.S. Hinkle, J. Org. Chem. 52 (1987) 4107–4110.
[15] J.M. Berlin, G.C. Fu, Angew. Chem. Int. Ed. 47 (2008) 7048–7050.
[16] (a) L. He, H. Lv, Y.-R. Zhang, S. Ye, J. Org. Chem. 73 (2008) 8101–8103;
(b) X.-N. Wang, P.-L. Shao, H. Lv, S. Ye, Org. Lett. 11 (2009) 4029–4031;
(c) Y.-R. Zhang, L. He, X. Wu, P.-L. Shao, S. Ye, Org. Lett. 10 (2008) 277–280;
(d) N. Duguet, C.D. Campbell, A.M.Z. Slawin, A.D. Smith, Org. Biomol. Chem. 6 (2008) 1108–1113;
(e) Y.-R. Zhang, H. Lv, D. Zhou, S. Ye, Chem. Eur. J. 14 (2008) 8473–8476;
(f) X.-L. Huang, L. He, P.-L. Shao, S. Ye, Angew. Chem. Int. Ed. 48 (2009) 192–195;
(g) X.-L. Huang, X.-Y. Chen, S. Ye, J. Org. Chem. 74 (2009) 7585–7587;
(h) N. Duguet, A. Donaldson, S.M. Leckie, J. Douglas, P. Shapland, T.B. Brown, G. Churchill, A.M.Z. Slawin, A.D. Smith, Tetrahedron Asymmetry 21 (2010) 582–600;
(i) N. Duguet, A. Donaldson, S.M. Leckie, E.A. Kallstrom, C.D. Campbell, P. Shapland, T.B. Brown, A.M.Z. Slawin, A.D. Smith, Tetrahedron Asymmetry 21 (2010) 601–616.
[17] (a) S. Yamabe, T. Minato, Y. Osamura, J. Chem. Soc. Chem. Commun. (1993) 450–452;
(b) S. Yamabe, K. Kuwata, T. Minato, Theor. Chem. Acc. 102 (1999) 139–146.
[18] (a) D.-H. Wei, M.-S. Tang, J. Zhao, L. Sun, W.-J. Zhang, C.-F. Zhao, S.-R. Zhang, H.-M. Wang, Tetrahedron Asymmetry 20 (2009) 1020–1026;
(b) L. Sun, M.-S. Tang, H.-M. Wang, D.-H. Wei, L.-L. Liu, Tetrahedron Asymmetry 19 (2008) 779–787;
(c) D.-H. Wei, M.-S. Tang, J. Phys. Chem. A 113 (2009) 11035–11041;
(d) J.-Y. Yuan, X.-C. Liao, H.-M. Wang, G.-Y. Yang, M.-S. Tang, J. Phys. Chem. B 113 (2009) 1418–1422;
(e) D.-H. Wei, W.-J. Zhang, Y.-Y. Zhu, M.-S. Tang, J. Mol. Catal. A: Chem. 326 (2010) 41–47.
[19] (a) M. Arno, R.J. Zaragoza, L.R. Domingo, Tetrahedron Asymmetry 18 (2007) 157–164;
(b) M. González-Béjar, S.-E. Stiriba, L.R. Domingo, J. Pérez-Prieto, M.A. Miranda, J. Org. Chem. 71 (2006) 6932–6941;
(c) L.R. Domingo, J. Andrés, J. Org. Chem. 68 (2003) 8662–8668;
(d) L.R. Domingo, A.J. Asensio, J. Org. Chem. 65 (2000) 1076–1083;
(e) L.R. Domingo, M. Arno, J. Saez, J. Org. Chem. 74 (2009) 5934–5940;
(f) L.R. Domingo, R. Perez-Ruiz, J.E. Arguello, M.A. Miranda, J. Phys. Chem. A 113 (2009) 5718–5722.
[20] (a) S. Fomine, J.V. Ortega, M.A. Tlenkopatchev, Organometallics 24 (2005) 5696–5701;
(b) S. Fomine, S.M. Vargas, M.A. Tlenkopatchev, Organometallics 22 (2003) 93–99;
(c) S. Fomine, J.V. Ortega, M.A. Tlenkopatchev, J. Mol. Catal. A: Chem. 263 (2007) 121–127;
(d) X. Zheng, P. Blowers, J. Mol. Catal. A: Chem. 246 (2006) 1–10.
[21] (a) N. Tsuchida, H. Satou, S. Yamabe, J. Phys. Chem. A 111 (2007) 6296–6303;
(b) S. Yamabe, S. Yamazaki, J. Org. Chem. 72 (2007) 3031–3041;
(c) S. Yamabe, S. Yamazaki, Org. Biomol. Chem. 7 (2009) 951–961.
[22] M.J. Frisch, G.W. Trucks, H.B. Schlegel, G.E. Scuseria, M.A. Robb, J.R. Cheeseman, J.A. Montgomery Jr., T. Vreven, K.N. Kudin, J.C. Burant, J.M. Millam, S.S. Iyengar, J. Tomasi, V. Barone, B. Mennucci, M. Cossi, G. Scalmani, N. Rega, G.A. Petersson, H. Nakatsuji, M. Hada, M. Ehara, K. Toyota, R. Fukuda, J. Hasegawa, M. Ishida, T. Nakajima, Y. Honda, O. Kitao, H. Nakai, M. Klene, X. Li, J.E. Knox, H.P. Hratchian, J.B. Cross, C. Adamo, J. Jaramillo, R. Gomperts, R.E. Stratmann, O. Yazyev, A.J.

Austin, R. Cammi, C. Pomelli, J.W. Ochterski, P.Y. Ayala, K. Morokuma, G.A. Voth, P. Salvador, J.J. Dannenberg, V.G. Zakrzewski, S. Dapprich, A.D. Daniels, M.C. Strain, O. Farkas, D.K. Malick, A.D. Rabuck, K. Raghavachari, J.B. Foresman, J.V. Ortiz, Q. Cui, A.G. Baboul, S. Clifford, J. Cioslowski, B.B. Stefanov, G. Liu, A. Liashenko, P. Piskorz, I. Komaromi, R.L. Martin, D.J. Fox, T. Keith, M.A. Al-Laham, C.Y. Peng, A. Nanayakkara, M. Challacombe, P.M.W. Gill, B. Johnson, W. Chen, M.W. Wong, C. Gonzalez, J.A. Pople, Gaussian 03, Revision C. 02, Gaussian, Inc., Wallingford CT, 2004.

[23] A.D. Becke, J. Chem. Phys. 98 (1993) 5648–5652.

[24] C. Lee, W. Yang, R.G. Parr, Phys. Rev. B 37 (1988) 785–789.

[25] C. Gonzalez, H.B. Schlegel, J. Chem. Phys. 90 (1989) 2154–2161.

[26] C. Gonzalez, H.B. Schlegel, J. Phys. Chem. 94 (1990) 5523–5527.

[27] V. Barone, M. Cossi, J. Phys. Chem. A 102 (1998) 1995–2001.

[28] B. Mennucci, J. Tomasi, J. Chem. Phys. 106 (1997) 5151–5158.

[29] (a) D.C. Fang, X.Y. Fu, Chin. Chem. Lett. 3 (1992) 367–368;
(b) B. Lecea, A. Arrieta, G. Roa, J.M. Ugalde, F.P. Cossio, J. Am. Chem. Soc. 116 (1994) 9613–9619;
(c) B. Lecea, A. Arrieta, X. Lopez, J.M. Ugalde, F.P. Cossio, J. Am. Chem. Soc. 117 (1995) 12314–12321;
(d) J.-M. Pons, A. Pommier, M. Rajzmann, D. Liotard, J. Mol. Struct. (Theochem.) 313 (1994) 361–364;
(e) J.-M. Pons, M. Oblin, A. Pommier, M. Rajzmann, D. Liotard, J. Am. Chem. Soc. 119 (1997) 3333–3338;
(f) X. Wang, K.N. Houk, J. Am. Chem. Soc. 112 (1990) 1754–1756.

[30] (a) R.G. Parr, R.G. Pearson, J. Am. Chem. Soc. 105 (1983) 7512–7516;
(b) L.R. Domingo, J.A. Saez, R.J. Zaragoza, M. Arno, J. Org. Chem. 73 (2008) 8791–8799;
(c) L.R. Domingo, M.J. Aurell, P. Perez, R. Contreras, Tetrahedron 58 (2002) 4417–4423;
(d) L.R. Domingo, J.A. Saez, R.J. Zaragoza, Org. Biomol. Chem. 7 (2009) 3576–3583;
(e) L.R. Domingo, M.T. Picher, J.A. Saez, J. Org. Chem. 74 (2009) 2726–2735;
(f) W. Kohn, L. Sham, J. Phys. Rev. 140 (1965) 1133–1138;
(g) L.R. Domingo, E. Chamorro, P. Perez, J. Phys. Chem. A 112 (2008) 4046–4053;
(h) L.R. Domingo, E. Chamorro, P. Perez, J. Org. Chem. 73 (2008) 4615–4624;
(i) C. Zhang, Y.-Y. Zhu, D.-H. Wei, D.-Z. Sun, W.-J. Zhang, M.-S. Tang, J. Phys. Chem. A 114 (2010) 2913–2919.